NANO LETTERS

Letter

pubs.acs.org/NanoLett

Improved Electrical Conductivity of Graphene Films Integrated with Metal Nanowires

Iskandar N. Kholmanov,[†,‡] Carl W. Magnuson,[†] Ali E. Aliev,[§] Huifeng Li,[†] Bin Zhang,[†] Ji Won Suk,[†] Li Li Zhang,[†] Eric Peng,[†] S. Hossein Mousavi,[∥] Alexander B. Khanikaev,[∥] Richard Piner,[†] Gennady Shvets,[∥] and Rodney S. Ruoff*[,†]

[†]Department of Mechanical Engineering and the Materials Science and Engineering Program, The University of Texas at Austin, 1 University Station C2200, Austin, Texas 78712, United States

[‡]CNR-IDASC Sensor Lab Department of Chemistry and Physics, University of Brescia, via Valotti, 9, Brescia 25133, Italy

[§]Alan G. MacDiarmid NanoTech Institute, University of Texas at Dallas, Richardson, Texas 75083, United States

[∥]Department of Physics and Center for Nano and Molecular Science and Technology, The University of Texas at Austin, Austin, Texas 78712, United States

Supporting Information

ABSTRACT: Polycrystalline graphene grown by chemical vapor deposition (CVD) on metals and transferred onto arbitrary substrates has line defects and disruptions such as wrinkles, ripples, and folding that adversely affect graphene transport properties through the scattering of the charge carriers. It is found that graphene assembled with metal nanowires (NWs) dramatically decreases the resistance of graphene films. Graphene/NW films with a sheet resistance comparable to that of the intrinsic resistance of graphene have been obtained and tested as a transparent electrode replacing indium tin oxide films in electrochromic (EC) devices. The successful integration of such graphene/NW films into EC devices demonstrates their potential for a wide range of optoelectronic device applications.

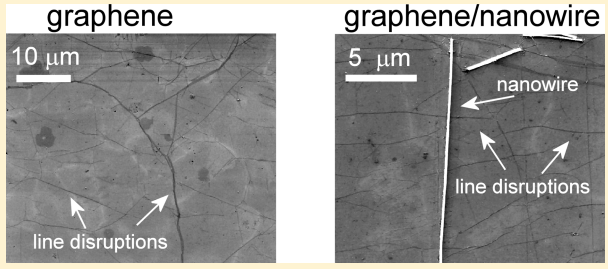

KEYWORDS: *Graphene, nanowires, transparent conductive films, electrochromic devices*

Due to low electron−phonon scattering, graphene has excellent transport properties with theoretical values of charge carrier mobility higher than 200 000 $cm^2/V{\cdot}s$.[1] In addition, single layer graphene absorbs about 2.3% of visible light.[2,3] The combination of these unique properties makes graphene an excellent candidate for transparent conductive films (TCF). Chemical vapor deposition (CVD) of hydrocarbon gases on metal surfaces allows scaling graphene films to large sizes that can be transferred onto arbitrary substrates.[4,5] These characteristics open the possibility to replace indium tin oxide (ITO) by graphene as the TCF, particularly for flexible and large-area device applications.

However, the sheet resistance (R_s) of CVD-grown monolayer graphene (>1 kΩ/sq)[6] is significantly higher than ITO-based TCFs. The charge carrier mobility in these graphene films is much lower[6] than mechanically exfoliated graphene[7,8] as well as theoretically calculated values.[1] Defects influence the transport properties of CVD-grown graphene. Large-area CVD-grown graphene is a polycrystalline material with topological defects such as dislocations and grain boundaries.[9−11] Grain boundaries in graphene are line defects at the interfaces between two domains with different crystallographic orientations.[9−12] Depending on the detailed atomic structure, these defects can disrupt the sp^2 delocalization of π electrons in graphene and effectively scatter the charge carriers.[10,12,13] This potential formation of highly resistive grain boundaries may lead to the carriers being trapped periodically in domains. Nanoripples, another line feature in CVD grown films, can also scatter charge carriers by the out-of-plane flexural phonons confined within the defects.[1,14] In addition to grain boundaries and nanoripples, a higher (than theoretical values[1]) electrical resistivity of the graphene can arise from other defects, such as point defects, wrinkles, folds, tears and cracks, and so forth, that can scatter the charge carriers resulting in decreased ballistic transport path length and carrier mobility.[15−17]

The electrical properties of graphene can be improved by minimizing the role of different defects. Some nonlinear structural defects in graphitic structures can be healed by high-temperature processing.[18,19] Growing a larger grain size graphene may result in some improvement in transport properties due to the lower density of grain boundaries.[13,20] However, to date these approaches have not yielded large-area single layer graphene films with a sheet resistance <100 Ω/sq

Received: August 2, 2012
Revised: October 2, 2012

   dx.doi.org/10.1021/nl302870x | *Nano Lett.* XXXX, XXX, XXX−XXX

required for some device applications. Recently, Jeong et al.[21] theoretically predicted that elimination of the detrimental effect of line defects can be achieved through the integration of CVD-grown graphene with one-dimensional (1D) metal nanowires (NWs). We demonstrate here experimentally the assembly of monolayer graphene with 1D metal NWs with the goal of minimizing the influence of line defects and line disruptions (the latter describes the wrinkles, ripples, and folding) on the transport properties of graphene films. Graphene/metal NW hybrid films with TCF characteristics comparable to that of ITO films (typically, R_s = 30−80 Ω/sq for an optical transmittance at λ = 550 nm (T_{550}) = 90%) were obtained and also tested as transparent electrodes in electrochromic devices to evaluate their possibly replacing the traditionally used ITO films.

Monolayer graphene was grown on polycrystalline Cu foil using a CVD technique described elsewhere.[6] A scanning electron microscope (SEM) image of a typical single layer graphene that continuously spans steps and facets of the Cu substrate is shown in Figure 1a. Line disruptions such as

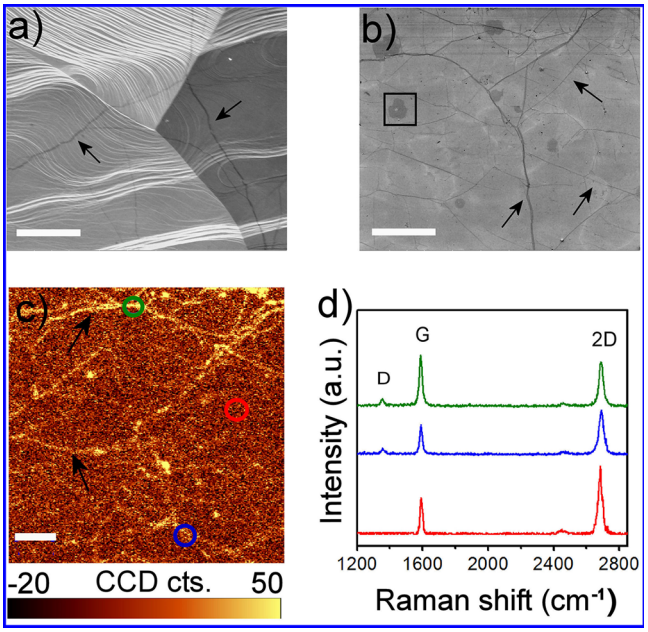

Figure 1. Characterization of CVD-grown graphene. (a) SEM image of graphene monolayer continuously grown across the grain boundaries and steps of a polycrystalline Cu substrate. (b) SEM image of graphene transferred onto a SiO_2/Si substrate. Dark islands, one of which is shown in the "squared" area, are bilayer graphene. (c) Raman map (1300−1400 cm^{-1}) centered on the D mode (1365 cm^{-1}). The arrows in a, b, and c show the line disruptions (such as wrinkles, ripples, and folding). Scale bars are 10 μm. (d) Raman spectra corresponding to the areas shown in the Raman map in (c) by blue, red, and green circles.

wrinkles, formed due to the difference in thermal contraction between graphene and the Cu substrate upon cooling,[4] can be easily seen in the SEM image. Transfer of graphene onto SiO_2/Si substrate substrates using a wet transfer method[6,22] (see also Supporting Information) results in a higher density of line disruptions (Figure 1b), indicating that the transfer process produces additional line disruptions in graphene films.

The line disruptions in the transferred graphene were also observed by Raman spectroscopy (WITEC Alpha300, λ = 532 nm, 100× objective). The Raman D band (~1365 cm^{-1}) of graphene is activated by the defects that cause an intervalley double resonance involving transitions near two inequivalent K points at neighboring corners of the first Brillouin zone of graphene.[23,24] A Raman map (1300−1400 cm^{-1}) around the D mode of graphene on a SiO_2/Si substrate shows bright lines corresponding to the line disruptions (Figure 1c). The spectra obtained on the bright lines (blue and green circles in Figure 1c) show the presence of the D peak (blue and green spectra in Figure 1d), in addition to the G and 2D modes centered at ~1575 cm^{-1} and ~2680 cm^{-1}, respectively. The intensity ratio of G and 2D modes in these spectra are different (I(2D)/I(G) ≈ 1.4 for blue and 0.9 for green), indicating the diversity of line disruptions. No detectable D peak was observed in the spectrum taken on the areas without bright lines (red circle in Figure 1c corresponding to red spectrum in Figure 1d). The latter spectrum is characterized by the intensity ratio of G and 2D modes (I(2D)/I(G) ≈ 2) and the full width at half-maximum (fwhm) of the 2D band (≈ 27 cm^{-1}) associated with single layer graphene.[23]

The sheet resistance of the graphene transferred onto glass substrates is as high as about 1.35 ± 0.14 kΩ/sq but decreases to about 1.05 ± 0.11 kΩ/sq after thermal treatment at 170 °C for 1 h in a vacuum chamber ($p < 2 \times 10^{-2}$ Torr). Integration of the graphene with Ag NWs is shown schematically in Figure 2a. Ag NW (average length and diameter of 5−25 μm and 100−130 nm, respectively) films on glass and SiO_2/Si substrates were obtained by spin coating NW dispersions in isopropyl alcohol with three different concentrations: 0.2 mg/mL, 0.6 mg/mL, and 1.0 mg/mL[25] (see Supporting Information). The corresponding films were denoted as NW1, NW2, and NW3, respectively. The films possess high optical transparency (T_{550} of about 98.6%, 97.2%, and 96.0%, respectively) that decreases with increasing NW concentration used to make the film. All of the NW films (NW1, NW2, and NW3) used in this work are nonconductive due to the subpercolation network of the NWs. Ag NW films above percolation may possess TCF characteristics comparable to ITO films.[26,27] Here, we targeted the subpercolation regime, where NWs can individually and locally improve the conductivity of graphene platelets but not provide their own global conductive path(s). This excludes the electrical conductivity of pure Ag NW films in the hybrid systems and allows considering the contribution of individual NWs (no network of NWs) in altering the electrical conductivity of the hybrid films.

Transfer of graphene onto Ag NW films was first performed by a dry transfer technique[22] (top processes shown in Figure 2a) that avoids trapping of the solutions (used in the transfer processes) near NWs (see Supporting Information). However, this transfer yielded graphene/Ag NW hybrid films in which most of the NWs were surrounded by suspended graphene (Figure 2b) that can be easily torn during integration into devices that would result in worsened transport properties of the hybrid film. To avoid the formation of the suspended graphene, a small amount of poly(methyl methacrylate) (PMMA) solution was drop-coated on top of the precoated PMMA/graphene/NW film (bottom processes in Figure 2a, denoted as "modified dry transfer"). This results in dissolving of the precoated PMMA and allows the PMMA/PMMA/graphene to better conform to the surface morphology of the underlying Ag NWs. After curing at room temperature for about 30 min, the PMMA was dissolved by acetone. In the

dx.doi.org/10.1021/nl302870x | Nano Lett. XXXX, XXX, XXX−XXX

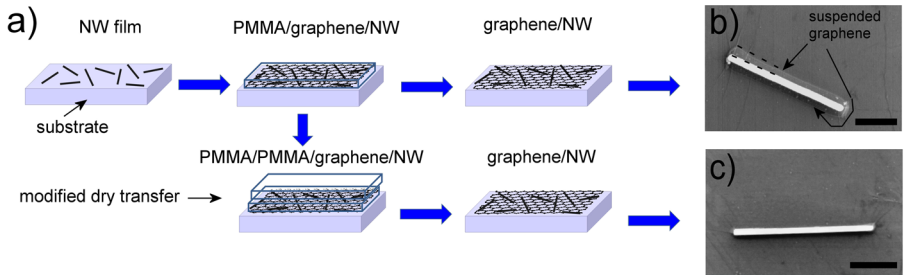

Figure 2. Fabrication of graphene/Ag NW films. (a) Schematic illustration of hybrid film fabrication. (b) SEM image of graphene dry transferred onto the NW film. Suspended graphene around the NW is shown by arrows. (c) Graphene/NW film after *modified dry transfer* process showing graphene conformal to the underlying NWs with no observable suspended graphene. Scale bars are 1 μm.

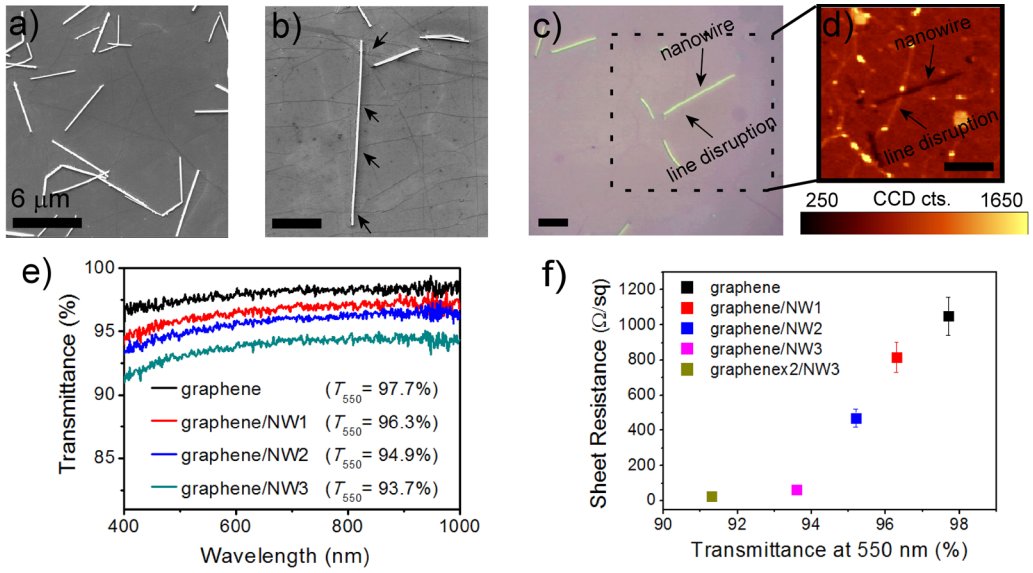

Figure 3. (a) Typical SEM image of graphene/NW films. (b) SEM image of a NW crossing several line disruptions shown by arrows. (c) Optical microscopy image of the hybrid films with a dashed line corresponding to the Raman map (1560−1620 cm^{-1}) showing a NW crossing with a line disruption in d. Scale bars in a, b, c, and d are 6 μm. (e) Optical transmittance spectra of graphene and graphene/NW films. (f) R_s versus optical transmittance for graphene and graphene/NW films.

obtained graphene/NW hybrid films no suspended graphene around the NWs has been observed as illustrated by the SEM image (Figure 2c). The graphene layer follows the curvature of the underlying NWs, providing larger interfacial contact area between graphene and NWs. This may enhance charge transfer between these two nanostructures thus improving the conductivity of the hybrid film.

A typical SEM image of the hybrid films produced by modified dry transfer method (Figure 3a) shows randomly oriented individual Ag NWs covered with a continuous 2D graphene layer. Figure 3b shows a NW crossing several line disruptions of the graphene layer. NW/line disruption crossings can also be seen in the Raman map (Figure 3d, corresponding to the dashed area in the optical microscopy image in Figure 3c). A Raman map (1500−1620 cm^{-1}) around the G mode of graphene on the SiO_2/Si substrate shows bright lines that correspond to the line disruptions and dark lines corresponding to the NWs (Figure 3c). The latter shows a lower intensity of Raman signal of graphene on top of the NWs.

The optical transmittance spectra of monolayer graphene and graphene/NW hybrid films presented in Figure 3e show higher than 90% transparency for all the films, which satisfies requirements for optical properties of transparent electrodes. The sheet resistance R_s was measured using the van der Pauw method after annealing the films at 170 °C for 1 h in a vacuum chamber ($p < 2 \times 10^{-2}$ Torr). Figure 3f shows that the R_s of the hybrid films decreases significantly with increasing concentration of Ag NWs for the films from NW1 to NW3. The lowest $R_s = 64 \pm 6.1$ Ω/sq with $T_{550} = 93.6\%$ was obtained for the graphene/NW3 films, significantly lower than that of pure graphene ($R_s = 1.05 \pm 0.11$ kΩ/sq). The obtained sheet resistance of the graphene/NW3 hybrid films is comparable to the intrinsic sheet resistance of "perfect" graphene (30 Ω/sq for graphene/SiO_2 system) that is due to solely electron−phonon scattering.[16] Taking into account the nonpercolative concentration of Ag NWs in the hybrid system and the role of the line defects (such as grain boundaries)[12] and line disruptions[14] to the graphene sheet resistance, the low R_s values obtained demonstrate that the Ag NWs bridge line defects and line disruptions and thus strongly reduces the electrical resistance of graphene. Metal NWs crossing the line disruptions (Figure 3b) and line defects[21] thus provide new conductive pathways for charge carriers in polycrystalline monolayer graphene. The SEM and Raman map (Figure 3b and 3d) show the Ag NWs bridging line disruptions; however some or many of the Ag NWs are also bridging the graphene line defects, as explained next. The length of Ag NWs reaches some tens of micrometers (Figure S1 in the Supporting Information), and the average size

dx.doi.org/10.1021/nl302870x | *Nano Lett.* XXXX, XXX, XXX−XXX

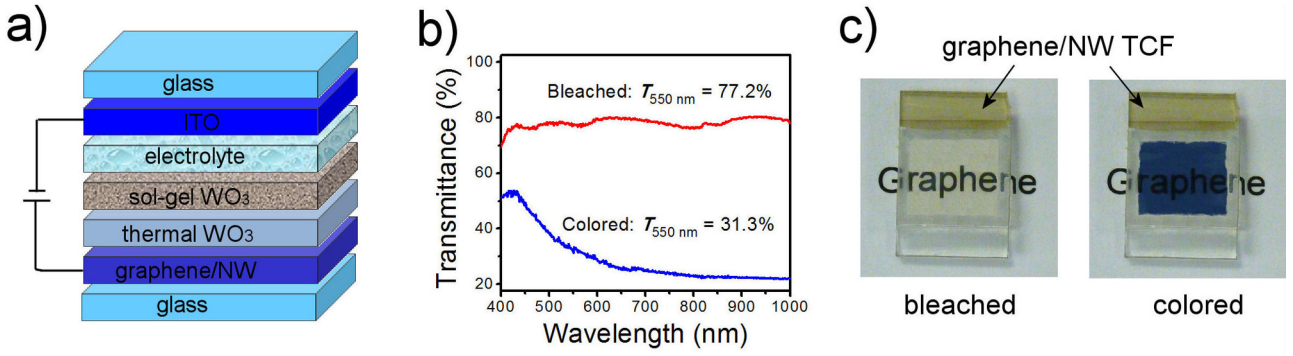

Figure 4. (a) Schematic illustration of an EC device structure. (b) Optical transmittance spectra of bleached and colored states of the EC device. (c) Photographs of the EC device in bleached and colored states with a background "Graphene". The graphene/NW transparent electrode with a conductive silver paste (yellow area) on top of the electrode is shown.

of graphene grains is about 10−12 μm (Figure S2 in Supporting Information). Thus, many of the Ag NWs covered by monolayer graphene bridge the graphene grain boundaries, and therefore, the obtained low sheet resistance values are due to the bridging by Ag NWs of both line disruptions and grain boundaries present in these graphene films.

The conductivity of the obtained graphene/NW films can be further improved while maintaining the $T_{550} > 90\%$. For example, adding a second graphene layer onto the graphene/NW3 yields a film with R_s = 24 (±3.6) Ω/sq for an optical transmittance of $T_{550} \approx 91\%$ (graphene × 2/NW3 in Figure 3f) that is better than doped four layer graphene-based (R_s = 30 Ω/sq with T_{550} = 90%)[5] films and ITO-based (R_s = 30−80 Ω/sq with T_{550} = 90%) films. Alternatively, NW films above percolation are likely to yield graphene/NW films with conductivity exceeding the intrinsic limit of ideal graphene, as has been demonstrated for graphene/metal grid systems.[28] These films are fundamentally different from that of the monolayer graphene/subpercolation NW films studied and described here. Namely, in this work the graphene film is the only conductive film component and the Ag NWs are an additional globally nonconductive component used to improve the conductivity of the graphene films. In contrast, in the hybrid systems with the percolated NW films or metal grids, the metal-component films are the main conductive constituent, and graphene is used as an additional conductive component to enhance the conductivity of the metal-component structures.

Doping has been studied as an alternative route to improve the conductivity of graphene,[5,29,30] as it can increase carrier densities, but doping does not directly address the adverse effects of line defects on conductivity. Doping of monolayer graphene films to achieve R_s < 100 Ω/sq has not to our knowledge been achieved. Doped graphene films are often of limited stability, such as films that have about a 40% increase in graphene sheet resistance within a few days.[31,32]

The graphene/NW films were tested as a transparent electrode in electrochromic (EC) devices. Typical EC devices are composed of an EC material and an electrolyte that are placed between two TCFs. During the electrochemical intercalation, induced by an external electric field applied between the two TCF electrodes, the injection and extraction of electrons and metal cations results in a modulation of optical properties of the EC layer.[33,34] In our experiments one of the two ITO TCFs was replaced by the graphene/NW TCFs on glass substrates (Figure 4a). Tungsten trioxide (WO3) films were used as the EC layer, and a propylene/ethylene carbonate solution (1:1) containing 1 M $LiClO_4$ was used as a Li-conductive electrolyte. It has been reported that sol−gel prepared nanostructured WO_3 films exhibit improved performance of EC devices with fast kinetics of the optical modulation.[34−36] However, direct deposition of sol−gel prepared WO_3 onto graphene/NW TCFs yields inhomogeneous films with poor morphologies. Therefore, a buffer layer of EC WO_3 with a thickness of approximately 100 nm was deposited onto the graphene/NW hybrid TCFs by thermal evaporation of WO_3 powder. Sol−gel WO_3 film with more attractive morphology for intercalation was spin coated on top of the buffer layer. The final double layer WO_3 thin films had a total thickness of about 500 nm. The complete EC device consisting of WO_3 EC layers and electrolyte placed between graphene/NW and ITO transparent electrodes on glass substrates is schematically shown in Figure 4a (see also Supporting Information).

Electrochemical reduction of WO_3 induced by external voltage (−3.0 V to the graphene/NW TCF) is accompanied with injection of electrons and intercalation of Li^+ ions into the EC layers and generation of W^{5+} sites. This results in an intense electrochromic absorption band due to the optically driven intervalence charge transfer between the W^{6+} and W^{5+} states and yields blue coloration of the EC films.[37] The "coloration" reaction can be written as:[37]

$$WO_3 + x[Li^+ + e^-] \rightarrow Li_xW^{+6}_{(1-x)}W^{+5}_xO^3$$

where x is the fractional number of sites in the WO_3 lattice that are filled by Li cations. The application of a reverse external field applied to the TCF electrodes extracts the Li cations and restores the bleached state of the EC film. The optical transmittance of the whole sandwich structure during coloration/bleaching cycles changes from T_{550} = 77.2% (bleached state) to T_{550} = 31.3% (colored state) as shown in Figure 4b. Stable coloration/bleaching processes are achieved after several initial cycles. The coloration and bleaching time for 90% transmittance change are 115 s and 205 s, respectively. These values are close to that of a EC device using the same sol−gel EC film, same electrolyte, but with two ITO electrodes.[35] The photograph images in Figure 4c show homogeneously bleached and colored states of the EC device. Repeatable cycling and homogeneous optical modulation of the tested devices demonstrates the successful performance of the graphene/NW films as a transparent electrode in EC devices.

In summary, line defects and line disruptions in transferred CVD-grown polycrystalline graphene films degrade their

dx.doi.org/10.1021/nl302870x | Nano Lett. XXXX, XXX, XXX−XXX

transport properties. We experimentally showed that graphene/NW assembly yields transparent conductive films with a sheet resistance (64 Ω/sq) slightly higher than the calculated intrinsic resistance of ideal graphene. The results demonstrate that the combination of graphene with 1D metal NWs can strongly reduce the overall resistance of the films. These hybrid films were successfully tested as a transparent electrode in electrochromic devices that show the coloration/bleaching characteristics comparable with EC devices using only ITO electrodes. The integration of such graphene/NW TCFs into EC devices demonstrates their potential for replacing ITO in a broad range of applications including displays, photovoltaics, and organic light-emitting diodes.

■ ASSOCIATED CONTENT

Supporting Information

Details of Ag NW film deposition, transfer of graphene, and EC device fabrication including the deposition of WO_3 films. This material is available free of charge via the Internet at http://pubs.acs.org.

■ AUTHOR INFORMATION

Corresponding Author

*E-mail: r.ruoff@mail.utexas.edu.

Notes

The authors declare no competing financial interest.

■ ACKNOWLEDGMENTS

This work was supported by a Tokyo Electron Ltd (TEL)-customized Semiconductor Research Corporation award (Project No.: 2009-OJ-1873—Development of graphene-based transparent conductive films for display applications). S.H.M., A.B.K., and G.S. would like to acknowledge the support from the Air Force Office of Scientific Research (FA9550-08-1-0394).

■ REFERENCES

(1) Morozov, S. V.; Novoselov, K. S.; Katsnelson, M. I.; Schedin, F.; Elias, D. C.; Jaszczak, J. A.; Geim, A. K. *Phys. Rev. Lett.* **2008**, *100*, 016602.

(2) Kuzmenko, B.; van Heumen, E.; Carbone, F.; van der Marel, D. *Phys. Rev. Lett.* **2008**, *100*, 117401.

(3) Nair, R. R.; Blake, P.; Grigorenko, A. N.; Novoselov, K. S.; Booth, T. J.; Stauber, T.; Peres, N. M. R.; Geim, A. K. *Science* **2008**, *320*, 1308.

(4) Li, X.; Cai, W.; An, J.; Kim, S.; Nah, J.; Yang, D.; Piner, R.; Velamakanni, A.; Jung, I.; Tutic, E.; Banerjee, S. K.; Colombo, L.; Ruoff, R. S. *Science* **2009**, *324*, 1312−1314.

(5) Bae, S.; Kim, H.; Lee, Y.; Xu, X.; Park, J.-S.; Zheng, Y.; Balakrishnan, J.; Lei, T.; Kim, H. R.; Song, Y. I.; Kim, Y.-J.; Kim, K. S.; Özyilmas, B.; Ahn, J.-H.; Hong, B. H.; Iijima, S. *Nat. Nanotechnol.* **2010**, *5*, 574−578.

(6) Li, X. S.; Zhu, Y. W.; Cai, W. W.; Borysiak, M.; Han, B. Y.; Chen, D.; Piner, R. D.; Colombo, L.; Ruoff, R. S. *Nano Lett.* **2009**, *9*, 4359−4363.

(7) Bolotin, K. I.; Sikes, K. J.; Jiang, Z.; Klima, M.; Fudenberg, G.; Hone, J.; Kim, P.; Stormer, H. L. *Solid State Commun.* **2008**, *146*, 351−355.

(8) Du, X.; Skachko, I.; Barker, A.; Andrei, E. Y. *Nat. Nanotechnol.* **2008**, *3*, 491−495.

(9) Huang, P. Y.; Ruiz-Vargas, C. S.; van der Zande, A. M.; Whitney, W. S.; Levendorf, M. P.; Kevek, J. W.; Garg, S.; Alden, J. S.; Hustedt, C. J.; Zhu, Ye.; Park, J.; McEuen, P. L.; Muller, D. A. *Nature* **2011**, *469*, 389−393.

(10) Yazyev, O. V.; Louie, S. G. *Nat. Mater.* **2010**, *9*, 806−809.

(11) Kim, K.; Lee, Z.; Regan, W.; Kisielowski, C.; Crommie, M. F.; Zettl, A. *ACS Nano* **2011**, *5*, 2142−2146.

(12) Song, H. S.; S. L. Li, S. L.; Miyazaki, H.; Sato, S.; Hayashi, K.; Yamada, A.; Yokoyama, N.; Tsukagoshi, K. *Sci. Rep.* **2012**, *2*, 337; DOI:10.1038/srep00337.

(13) Yu, Q.; Jauregui, L. A.; Wu, W.; Colby, R.; Tian, J.; Su, Z.; Cao, H.; Liu, Z.; Pandey, D.; Wei, D.; Chung, T. F.; Peng., P.; Guisingers, N. P.; Stach, E. A.; Bao, J.; Pei, S.-S.; Chen, Y. P. *Nat. Mater.* **2011**, *10*, 443−449.

(14) Ni, G. X.; Zheng, Y.; Bae, S.; Kim, H. R.; Pachoud, A.; Kim, Y. S.; Tan, C. L.; Im, D.; Ahn, J. H.; Hong, B. H.; Ozyilmaz, B. *ACS Nano* **2012**, *6*, 1158−1164.

(15) Kim, K.; Park, H. J.; Woo, B.-C.; Kim, K. J.; Kim, G. T.; Yun, W. S. *Nano Lett.* **2008**, *8*, 3092−3096.

(16) Chen, J. H.; Jang, C.; Xiao, S. D.; Ishigami, M.; Fuhrer, M. S. *Nat. Nanotechnol.* **2008**, *3*, 206−209.

(17) Gannett, W.; Regan, W.; Watanabe, K.; Taniguchi, T.; Crommie, M. F.; Zettl, A. *Appl. Phys. Lett.* **2011**, *98*, 242105.

(18) Kholmanov, I. N.; Edgeworth, J.; Cavaliere, E.; Gavioli, L.; Magnuson, C.; Ruoff, S. R. *Adv. Mater.* **2011**, *23*, 1675−1678.

(19) Karoui, S.; Amara, H.; Bichara, C.; Ducastelle, F. *ACS Nano* **2010**, *4*, 6114−6120.

(20) Li, X. S.; Magnuson, C. W.; Venugopal, A.; An, J.; Suk, J. W.; Han, B.; Borysiak, M.; Cai, W.; Velamakanni, A.; Zhu, Y.; Fu, L.; Vogel, E. M.; Voelkl, E.; Colombo, L.; Ruoff, R. S. *Nano Lett.* **2010**, *10*, 4328−4334.

(21) Jeong, C.; Nair, P.; Khan, M.; Lundstrom, M.; Alam, M. A. *Nano Lett.* **2011**, *11*, 5020−5025.

(22) Suk, J. W.; Kitt, A.; Magnuson, C. W.; Hao, Y.; Ahmed, S.; An, J.; Swan, A. K.; Goldberg, B. B.; Ruoff, R. S. *ACS Nano* **2011**, *5*, 6916−6924.

(23) Ferrari, A. C. *Solid State Commun.* **2007**, *143*, 47−57.

(24) Ding, F.; Ji, H. X.; Chen, Y. H.; Herklotz, A.; Dorr, K.; Mei, Y. F.; Rastelli, A.; Schmidt, O. G. *Nano Lett.* **2010**, *10*, 3453−3458.

(25) Kholmanov, I. N.; Stoller, M.; Edgeworth, J.; Lee, W. H.; Li, H.; Lee, J.; Barnhart, C.; Potts, J.; Piner, R.; Akinwande, D.; Barrick, J. E.; Ruoff, R. S. *ACS Nano* **2012**, *6*, 5157.

(26) Hu, L.; Kim, H. S.; Lee, J. Y.; Peumans, P.; Cui, Y. *ACS Nano* **2010**, *4*, 2955−2963.

(27) Garnett, E. C.; Cai, W.; Cha, J. J.; Mahmood, F; Connor, S. T.; Christoforo, M. G.; Cui, Y.; McGehee, M. D.; Brongersma, M. L. *Nat. Mater.* **2012**, *11*, 241−249.

(28) Zhu, Y.; Sun, Z.; Yan, Z.; Jin, Z.; Tour, J. M. *ACS Nano* **2011**, *5*, 6472−6479.

(29) Blake, P.; Brimicombe, P. D.; Nair, R. R.; Booth, T. J.; Jiang, D.; Schedin, F.; Ponomarenko, L. A.; Morozov, S. V.; Gleeson, H. F.; Hill, E. W.; et al. *Nano Lett.* **2008**, *8*, 1704−1708.

(30) Han, T. H.; Lee, Y.; Choi, M. R.; Woo, S. H.; Bae, S. H.; Hong, B. H.; Ahn, J. H.; Lee, T. W. *Nat. Photon.* **2012**, *6*, 105−110.

(31) Ni, G. X.; Zheng, Y.; Bae, S.; Tan., C. Y.; Kahya, O.; Wu, J.; Hong, B. H.; Yao, K.; Ozyilmaz, B. *ACS Nano* **2012**, *6*, 3935−3942.

(32) Yan, C.; Kim, K. S.; Lee, S. K.; Bae, S. H.; Hong, B. H.; Kim, J. H.; Lee, H. J.; Ahn, J. H. *ACS Nano* **2012**, *6*, 2096−2103.

(33) Granqvist, C. G.; Niklasson, G. A.; Azens, A. *Appl. Phys. A: Mater. Sci. Process.* **2007**, *89*, 29−35.

(34) Deepa, M.; Srivastava, A. K.; Kar, M.; Agnihotry, S. A. *J. Phys. D: Appl. Phys.* **2006**, *39*, 1885−1893.

(35) Aliev, A. E.; Shin, H. W. *Solid State Ionics* **2002**, *154*−*155*, 425−431.

(36) Krašovec, U. O.; Topič, M.; Georg, A.; Georg, A.; Dražič, G. *J. Sol-Gel Sci. Technol.* **2005**, *36*, 45−52.

(37) Somani, P. R.; Radhakrishnan, S. *Mater. Chem. Phys.* **2002**, *77*, 117−133.